J. Fluid Mech. (1990), *vol.* 221, *pp.* 131–159
Printed in Great Britain

Response of a turbulent boundary layer to sinusoidal free-stream unsteadiness

By G. J. BRERETON†, W. C. REYNOLDS AND R. JAYARAMAN‡
Department of Mechanical Engineering, Stanford University, Stanford, CA 94305, USA

(Received 11 May 1988 and in revised form 19 April 1990)

In this paper, selected findings of a detailed experimental investigation are reported concerning the effects of forced free-stream unsteadiness on a turbulent boundary layer. The forced unsteadiness was sinusoidal and was superimposed locally on an otherwise-steady mainstream, beyond a turbulent boundary layer which had developed under constant-pressure conditions. Within the region over which free-stream unsteadiness was induced, the sinusoidal variation in pressure gradient was between extremes of zero and a positive value, with a positive average level. The local response of the boundary layer to these free-stream effects was studied through simultaneous measurements of the u- and v-components of the velocity field.

Although extensive studies of unsteady, turbulent, fully-developed pipe and channel flow have been carried out, the problem of a developing turbulent boundary layer and its response to forced free-stream unsteadiness has received comparatively little attention. The present study is intended to redress this imbalance and, when contrasted with other studies of unsteady turbulent boundary layers, is unique in that: (i) it features an appreciable amplitude of mainstream modulation at a large number of frequencies of forced unsteadiness, (ii) its measurements are both detailed and of high spatial resolution, so that the near-wall behaviour of the flow can be discerned, and (iii) it allows local modulation of the mainstream beyond a turbulent boundary layer which has developed under the well-known conditions of steady, two-dimensional, constant-pressure flow.

Results are reported which allow comparison of the behaviour of boundary layers under the same mean external conditions, but with different time dependence in their free-stream velocities. These time dependences correspond to: (i) steady flow, (ii) quasi-steadily varying flow, and (iii) unsteady flow at different frequencies of mainstream unsteadiness. Experimental results focus upon the time-averaged nature of the flow; they indicate that the mean structure of the turbulent boundary layer is sufficiently robust that the imposition of free-stream unsteadiness results only in minor differences relative to the mean character of the steady flow, even at frequencies for which the momentary condition of the flow departs substantially from its quasi-steady state. Mean levels of turbulence production are likewise unaffected by free-stream unsteadiness and temporal production of turbulence appears to result only from modulation of the motions which contribute to turbulence production as a time-averaged measure.

---

† Present address: Department of Mechanical Engineering and Applied Mechanics, The University of Michigan, Ann Arbor, Michigan.
‡ Present address: IBM Research Division, Thomas J. Watson Research Center, New York.

1. Introduction

Turbulent boundary layers developing under time-dependent free-stream conditions are of great engineering importance, particularly in the fields of aerodynamics and turbomachinery. Yet, in contrast to the wealth of knowledge about their steady counterparts, information on the behaviour of unsteady turbulent boundary layers is scarce. Lighthill (1954) has provided an analytical framework within which the related laminar boundary-layer problem may be treated (for the case of small oscillations of external velocity about a steady mean) and Patel (1975) has extended this work to include laminar boundary-layer response to disturbances in the form of a travelling wave. While Patel (1977) and Cebeci (1977) have also considered computational solutions of the related turbulent problem using mixing-length and eddy-viscosity formulations, experimental support is needed for improved understanding of these flows. It is necessary for the purposes of examining the nature of turbulence in unsteady boundary layers and for addressing the growing needs of turbulence modellers for target data.

To date, studies of turbulent boundary layers growing under unsteady free-stream conditions have been predominantly experimental in nature and the case of a wall-bounded flow with a sinusoidally-varying mainstream is the one most commonly investigated. The experiments reported by Karlsson (1959), Patel (1977), and Cousteix & Houdeville (1983) concerned the behaviour of the boundary layer when there was no mean pressure gradient. The corresponding flow with an imposed mean gradient in pressure was examined by Schachenmann & Rockwell (1976), Kenison (1977), Cousteix & Houdeville (1983) and Simpson, Shivaprasad & Chew (1983). A general conclusion reached in all these studies was that time-averaged velocity and turbulence measurements appeared insensitive to variation in the frequency of unsteadiness imposed on the flow. However, while further insights into the behaviour of turbulent boundary layers were revealed in each study, it was not clear that a deduction made from any one experiment would apply to another. The conditions under which the boundary layer developed, upstream of the measurement stations, varied in each case.

Time-dependent, fully-developed, turbulent internal flows have also received considerable attention through both experimental and computational efforts. The detailed investigations of Tu & Ramaprian (1983) and Ramaprian & Tu (1983) into periodic, turbulent pipe flow have served as target data for numerical predictions employing a variety of turbulence models, such as those of Kebede, Launder & Younis (1985) and Blondeaux & Colombini (1985). The studies of Mizushina *et al.* (1973, 1975) have addressed issues of stuctural information concerning these flows. Also, effects of periodic through-flow rates in fully-developed channel flow have been studied by Acharya & Reynolds (1975), Binder *et al.* (1985) and Tardu, Binder & Blackwelder (1987).

A review of the aforementioned studies reveals inconsistencies, both in the conclusions which were drawn and in the way in which they were reached. While the results of some investigations indicated that the time-averaged unsteady flow was no different from steady flow under the same mean free-stream conditions, other studies have indicated that subtle differences were present. Conflicting results such as these have arisen through comparisons of time-averaged unsteady measurements with both steady measurements, made *in situ*, and with reference measurements/results from related experiments conducted under similar conditions. The same difficulty has been noted in studies of differences between the behaviour of unsteady flow and

quasi-steady flow (flow in which unsteadiness is characterized by extremely long timescales, and in which the momentary state may be described at any time by a steady flow with the same external conditions). While quasi-steady behaviour was deduced by direct measurement in some studies, in others it was necessary to synthesize this behaviour through superposition of reference measurements/functions, assumed to describe the quasi-steady flow accurately at each discrete phase during the time-dependent cycle. While this inconsistency is common to studies of developing and fully-developed flows alike, for the case of a developing turbulent boundary layer in unsteady flow, the variety of upstream conditions present in different experiments has resulted in uncertainty in the generality of conclusions drawn from any one study. These shortcomings have both complicated comparison of results of different experiments and hindered correct interpretation of the behaviour of the unsteady turbulent boundary layer and the present investigation has been carefully tailored to avoid these drawbacks.

2. Objectives

An important objective of this study was to conduct an experiment which focused on effects of unsteadiness upon a well-developed turbulent boundary layer. The apparatus was therefore designed so that a two-dimensional flat-plate turbulent boundary layer would develop under steady conditions and only locally, in a region downstream of the developed boundary layer, would sinusoidal unsteadiness be superimposed on an otherwise steady free stream. Thus, effects which might further complicate understanding of the flow, such as laminar–turbulent transition of the developing boundary layer under unsteady conditions, would not be present in this experiment.

In the pursuit of this objective, another benefit of growing the test boundary layer under steady constant-pressure conditions became clear – the net spanwise vorticity of the layer would remain constant during development and would arise solely as a result of the (steady) pressure gradient at the leading edge from which it was initiated. This point is clearer if one considers that the ensemble-average x-momentum equation at a solid surface may be written *exactly* as:

$$\nu \frac{\partial \langle \omega_3 \rangle}{\partial y} = \frac{1}{\rho} \frac{\partial \langle p \rangle}{\partial x}, \tag{1}$$

where ω_3 represents the spanwise component of vorticity. Thus, in this study, unsteady spanwise vorticity would be generated only locally, in a region downwind of a well-developed turbulent boundary, where an unsteady pressure gradient would be induced. In contrast, in experiments such as those reported in Cousteix & Houdeville (1983), the entire flow was periodic and there was both unsteady generation of boundary-layer vorticity at the leading-edge (which was subsequently convected downstream), and local creation of vorticity at the surface owing to the unsteady pressure gradient. From a simple vorticity-integral analysis (Brereton & Reynolds 1987), it could be shown that the reinforcement and cancellation of vorticity from these two sources manifested itself in the spatially-periodic values of δ^* and θ observed by Cousteix & Houdeville (1983) during the development of their boundary layer. If the response of boundary-layer turbulence to forced unsteadiness is to be studied in isolation from effects of: (i) boundary-layer development under unsteady conditions, and (ii) convection of unsteady leading-edge vorticity, the objective of conducting an experiment under steady upstream conditions is of

considerable importance. Moreover, a steady, two-dimensional, flat-plate boundary layer provides a well-known initial condition from which turbulence modellers might begin time-dependent predictions of the unsteady flow downstream.

A further objective of this study was to impose free-stream unsteadiness over a sufficiently wide range of frequencies so as to encompass some timescales of interest in unsteady, turbulent, boundary-layer flow. The range was chosen so that the lowest frequency would correspond to the approach of $\tilde{u}$ (the periodic component of streamwise velocity, according to the triple decomposition of Hussain & Reynolds 1970) to its quasi-steady asymptote, while the highest one would correspond to a frequency at which the asymptotic high-frequency behaviour of $\tilde{u}$ had been reached. Together with the unsteady response of the boundary layer, the quasi-steady response and the character of the steady boundary layer were to be measured at the mean condition of the unsteady mainstream. Simultaneous measurements of the u- and v-components of velocity were to be made with a two-colour laser-Doppler anemometer. Through the use of beam expansion, satisfactory resolution would be sought to allow near-wall behaviour to be discerned. A final objective was to ensure that an appreciable amplitude of mainstream unsteadiness was superimposed locally on the otherwise steady free stream, so that good signal-to-noise ratios would be achieved in unsteady components of turbulence measurements.

3. Details of the experiments

3.1. *Apparatus*

The experiments were performed in a closed-loop water tunnel (figure 1), the performance of which was tested thoroughly in a preliminary study by Jayaraman, Parikh & Reynolds (1982). Water flowed into the tunnel from a constant-head tank, the level within which was maintained precisely by an overflow weir positioned some 3.4 m above the point of exit from the water tunnel to a sump. From the constant-head tank, water flowed to the inlet of a two-dimensional contraction (20:1), via a honeycomb section and three taut screens of 70% porosity. At the contraction exit, the flow entered a horizontal duct of rectangular cross-section (0.15 m high and 0.35 m wide) – the *development section*. Here a new turbulent boundary layer was tripped on the top wall and developed for 2.0 m as a flat-plate turbulent boundary layer. The increasing blockage effect of this layer was compensated for by bleeding off, along the bottom wall, sufficient flow to maintain a constant free-stream velocity. At the end of the development section, the turbulent boundary layer was characterized by a Reynolds number (Re_θ) of 3200 and had developed with a free-stream velocity of 0.74 m/s.

Immediately downstream of the development section was the *test section*, shown in schematic form in figure 2. Water which entered the test section exited to the sump by one of the two routes shown through the porous bottom surfaces which led to adjacent but separated ducts. A sliding (motor-driven) plate with several longitudinal slots acted as a gate valve, which controlled flow from both ducts. The area of these slots was, by design, the controlling resistance to flow from the overhead tank to the sump. As the gate valve was moved, the fractional area seen by either duct varied in proportion to the valve's position while the total area presented to the two exiting flows remained constant (and thus maintained steady conditions upstream).

The porous surfaces comprised arrays of uniformly-spaced holes in flat plates; within the test section, flow exiting through this surface would cause a nearly linear

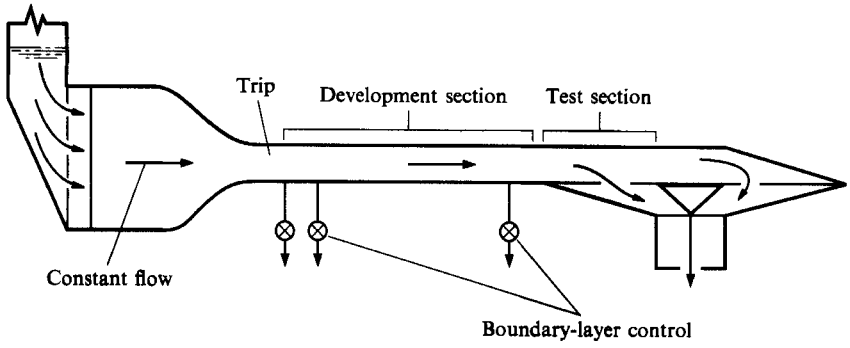

FIGURE 1. Closed-loop water tunnel.

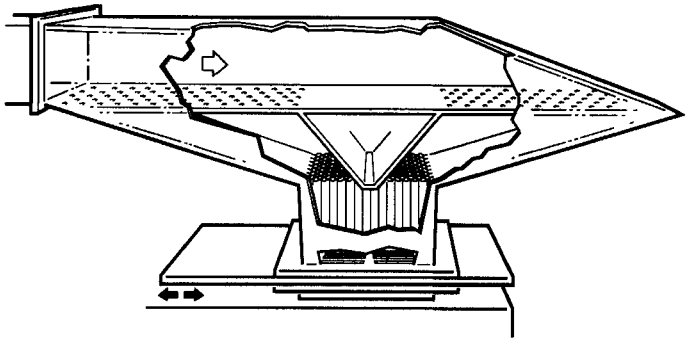

FIGURE 2. Test section of the water tunnel.

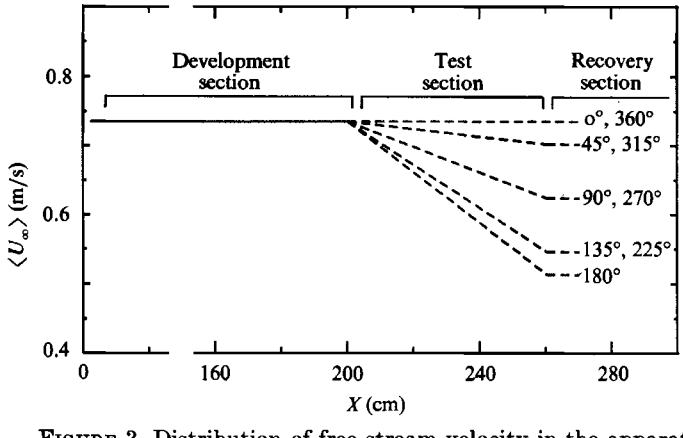

FIGURE 3. Distribution of free-stream velocity in the apparatus.

decrease in the free-stream velocity along it. Thus sinusoidal movement of the sliding plate caused the test free-stream velocity to oscillate about its mean value. During any cycle, the mean streamwise pressure gradient was positive and its lowest momentary value (no flow through the bottom surface) corresponded to constant pressure flow (illustrated in figure 3). The time dependence of the mainstream, at any streamwise position in the test section, was therefore of the form:

$$\langle u_\infty \rangle = U_0(1-A)+U_0 A\cos\omega t. \tag{2}$$

Here U_0 is the steady free-stream velocity upstream of the test section, A is the local amplitude of oscillation, expressed as a fraction of U_0, and U_∞ (the local mean free-stream velocity) is then $U_0(1-A)$. The free-stream velocity at any phase in the time-dependent cycle is represented by $\langle u_\infty \rangle$. For a wall-bounded flow with the free stream described by (2), it is apparent that the problem of interaction between vorticity created locally at the test surface (due to the unsteady test-section pressure gradient) and vorticity convected from regions upstream within the test section (created by the unsteady pressure gradient there), would persist. However a vorticity-integral analysis (referred to in §2) indicated that the local effect of this interaction was an order of magnitude smaller than the amplitude of the boundary-layer vorticity owing to the local unsteady pressure gradient, at all streamwise positions in the test section. Furthermore, in the preliminary experiments conducted by Jayaraman *et al.* (1982) in this apparatus, no spatial periodicity could be detected in measures of δ^* and θ.

Simultaneous measurements of the u- and v-components of the velocity field were made within the boundary layer on the top wall of the test section, with a two-colour laser-Doppler anemometer operated in forward-scatter mode, 15° off axis. With the inclusion of a beam expander (3.75×) in the transmitting optics, the length (in the spanwise direction, relative to the apparatus) and diameter of the probe volumes were reduced to about 1.5 mm and 0.15 mm respectively. Spanwise resolution was improved by an additional factor of three through the use of a field-stop system positioned in front of the receiving optics. At the measurement station for which results are reported in this study, the approximate dimensions of the measuring volume corresponded to 8.3 viscous units in length and 2.5 viscous units in diameter. Frequency shifting was employed in both channels and the downmixed Doppler signals were monitored by frequency trackers. Details of this measurement system and the qualification tests performed on it are described by Brereton & Reynolds (1987).

The use of a frequency-shifted forward-scatter system in water ensured that data could be tracked at a high rate (around 4000 Hz – an order of magnitude greater than the Kolmogorov frequencies, estimated at 100 Hz, and considerably higher than the fastest desired sampling rates). There was no indication of signal drop-out and so the output voltages of the two frequency trackers were considered continuous. They were sampled simultaneously, at 512 evenly spaced times per cycle, each of which was conditioned on the phase of the sliding valve which forced the sinusoidal variation in free-stream velocity. The periodic nature of the flow allowed successive cycles to be considered as independent events. Therefore ensembles of measurements, made at the same phase in many cycles, could be used to deduce the phase-averaged values of quantitites, which are represented as $\langle u \rangle$, $\langle -u'v' \rangle$ *etc.* In these experiments, 500 ensembles at each of 512 phases were sufficient to ensure repeatability in measurements. The quantity which proved most difficult to measure accurately and repeatably with this number of ensembles was $\langle -u'v' \rangle$. For typical values of this quantity, the relative uncertainty was assessed as ±7% with a 95% confidence level.

3.2. *Decomposition and averaging*

The triple decomposition of Hussain & Reynolds (1970) was used to describe the time-dependent, turbulent behaviour of the general dependent variable, $f(\boldsymbol{x},t)$, which could be expressed as the summed contribution of three parts:

$$f(\boldsymbol{x},t) = \bar{f}(\boldsymbol{x},t) + \tilde{f}(\boldsymbol{x},t) + f'(\boldsymbol{x},t). \tag{3}$$

Boundary layer parameter	Value
Free-stream velocity (U_0)	740 mm/s
Boundary-layer thickness (D_c)†	39.9 mm
Displacement thickness (δ^*)	6.8 mm
Momentum thickness (θ)	4.7 mm
Shape factor (H)	1.44
Momentum-thickness Reynolds number (Re_θ)	3190
Friction coefficient (C_f)	3.02×10^{-3}
Kinematic viscosity (ν)	1.1×10^{-6} m^2/s
Temperature	16.7 °C

† D_c is the boundary-layer thickness deduced from a least-squares fit of Coles' mean velocity function (Coles 1968).

TABLE 1. Test section inlet conditions

These components are the mean or time-averaged one, the deterministic or periodic one, and the turbulent component respectively. In order to separate any variable into these components, two averaging procedures were required and these were: (i) the phase average or ensemble average:

$$\langle f(\boldsymbol{x},t)\rangle = \lim_{N\to\infty} \frac{1}{N} \sum_{n=0}^{N-1} f(\boldsymbol{x}, t+n\tau), \tag{4}$$

where τ is the period of the cycle, and (ii) the time average:

$$\bar{f}(\boldsymbol{x}) = \lim_{N\to\infty} \frac{1}{N} \sum_{n=0}^{N-1} f(\boldsymbol{x}, t_0+n\Delta t) \quad \text{where} \quad N\Delta t \gg \tau. \tag{5}$$

It follows that:

$$\left.\begin{aligned} \langle f(\boldsymbol{x},t)\rangle &= \bar{f}(\boldsymbol{x}) + \tilde{f}(\boldsymbol{x},t), & f'(\boldsymbol{x},t) &= f(\boldsymbol{x},t) - \langle f(\boldsymbol{x},t)\rangle, \\ \overline{\langle f(\boldsymbol{x},t)\rangle} &= \bar{f}(\boldsymbol{x}), & \tilde{f}(\boldsymbol{x},t) &= \langle f(\boldsymbol{x},t)\rangle - \overline{\langle f(\boldsymbol{x},t)\rangle}. \end{aligned}\right\} \tag{6}$$

Using this decomposition, equations of fluid motion may be devised for each of the mean, periodic and turbulent fields of flow. Experimental measurements may be decomposed in the same fashion and turbulent flow oscillating about some mean condition may then be examined according to the behaviour of each of three components in its respective field.

3.3. *Qualification measurements*

Preliminary tests were performed to ensure that the design of the apparatus was satisfactory – that the sensitivity of upstream conditions to downstream disturbances was acceptably low and that spanwise variation in any measure was minimal. When the sliding valve of the test section was motored back and forth in an oscillatory manner, there was a slight upstream disturbance. However, this induced variation in $\langle U_0\rangle$, the free-stream velocity in the development section, was always less than 1.5% (r.m.s.) of its mean value. Measurements of the background level of free-stream turbulence in the development section were also made; at no location did it exceed 0.2%. In addition, surveys of the uniformity of quantities such as $\langle u\rangle$ and $\langle -u'v'\rangle$ across the span of the tunnel revealed that their variation was a small percentage of representative mean values (typically $\leqslant 2\%$). From these measurements it was inferred that the upstream flow scarcely differed from a standard, flat-plate, turbulent boundary layer and was virtually unaffected by

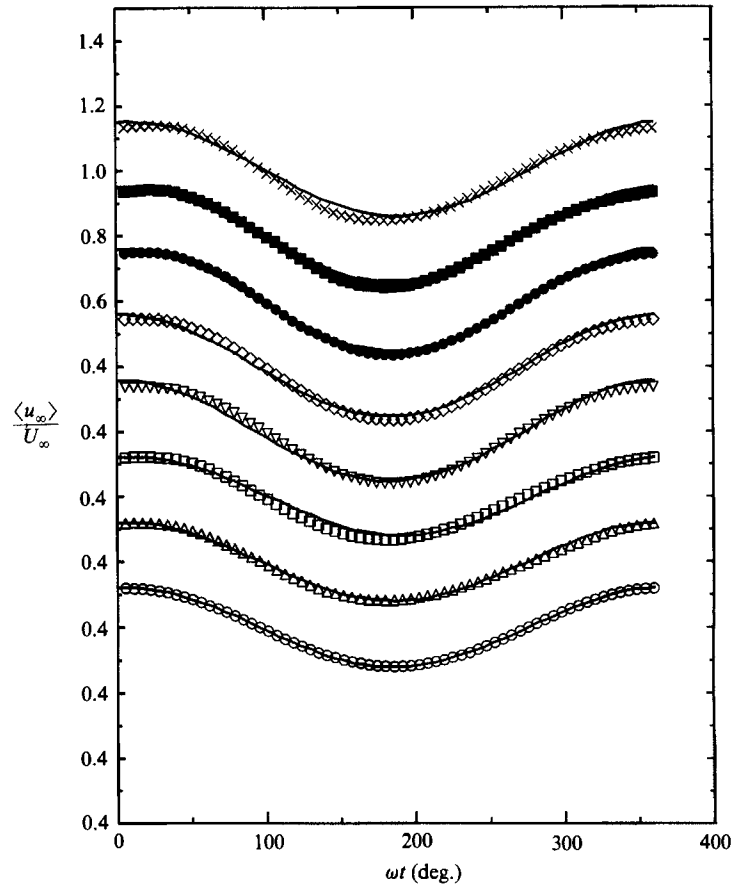

FIGURE 4. Variation of $\langle u_\infty \rangle$ with phase angle. ——, $1+(A/1-A)\cos\omega t$; ○, quasi-steady; △, 0.1 Hz; □, 0.2 Hz; ▽, 0.5 Hz; ◇, 0.8 Hz; ●, 1.0 Hz; ■, 1.6 Hz; ×, 2.0 Hz. Note the shifted ordinate; the uppermost graph corresponds to the uppermost numerical legends.

oscillatory behaviour in the test section. Characteristic parameters of this boundary layer are shown in table 1.

The corresponding time dependence of the free-stream velocity, at a measurement station within the test section, is shown in figure 4. It is evident that the oscillatory motion of the sliding valve produced a good representation of sinusoidal variation in mainstream velocity over the range of frequencies considered. The small degree of asymmetry about the reference sine wave at high frequencies was caused by imperfections in the flow-control system, as were minor variations in the imposed amplitude. When the data of figure 4 were decomposed into Fourier modes, the energy content at the fundamental frequency accounted for more than 99% of the total harmonic content in each case, indicating that the desired free-stream boundary condition (equation (2)) had been effectively achieved.

The distributions of free-stream velocity measured in the test section of the experimental apparatus are shown in figure 5(*a*, *b*). The linearity of the streamwise variation in $\langle u_\infty \rangle$ is demonstrated in figure 5(*a*), in which free-stream velocity is plotted as a function of phase angle at selected locations along the test section. All data presented in this figure were measured at the same distance from the wall, 1.7 times the boundary-layer thickness at the entrance to the test section (δ_0). A

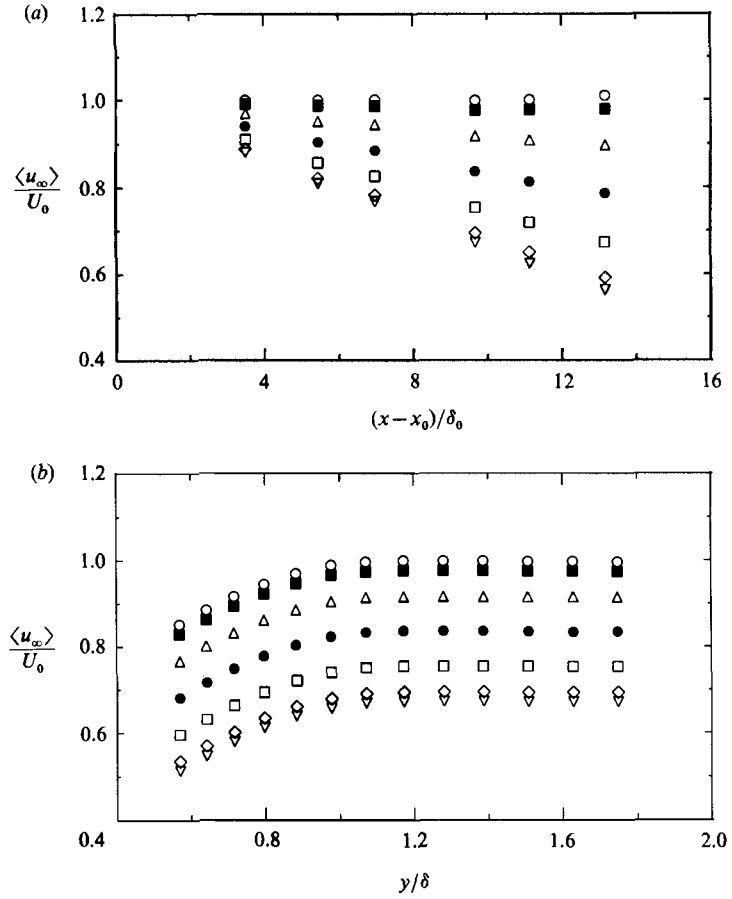

FIGURE 5. (*a*) Variation of $\langle u_\infty \rangle / U_0$ with phase angle along the test section, for oscillation at 1.0 Hz. ○, 0°; △, 60°; □, 120°; ▽, 180°; ◇, 210°; ●, 270°; ■, 330°. Note that δ_0 and U_0 are the free-stream velocity and boundary-layer thickness at the entrance to the test section. (*b*) Variation of $\langle u_\infty \rangle / U_0$ with phase angle in the outer boundary layer and free stream, for oscillation at 1.0 Hz. ○, 0°; △, 60°; □, 120°; ▽, 180°; ◇, 210°; ●, 270°; ■, 330°.

representative frequency of 1.0 Hz was chosen at which to show these data though measurements at other frequencies were qualitatively no different. The wall-normal uniformity of the time-dependent free stream at the principal measurement location ($(x-x_0)/\delta_0 = 9.63$, where δ_0 is given in table 1) is shown in figure 5(*b*), for oscillation at 1.0 Hz. It is clear that the method of flow control employed in this apparatus resulted in a free stream which was quite uniform beyond the boundary layer as far from the wall as measurements were made. These most distant measurements were made at the mid-point of the channel, nearly two boundary-layer thicknesses beyond the top wall. Comparable uniformity was noted at all other measurement stations and at all other frequencies of unsteadiness. It therefore appeared that the time-dependent free stream was a good representation of the desired external velocity distribution in phase, amplitude and linearity. Qualification aspects of these kinds are addressed in more detail by Jayaraman *et al.* (1982); in that study, particular emphasis was placed on demonstrating that the forcing external velocity was effectively in phase at all streamwise locations along the test section and so could not be considered a travelling wave.

Sets of velocity measurements were made across the boundary layer at three different x-locations and all those presented in this paper were taken at a single station, approximately two-thirds of the way along the test section. At this measurement station, A took the nominal value of 0.15. In practice, imperfections in the flow-control mechanism caused A to vary between 0.149 and 0.157 depending on the frequency at which the flow-control mechanism was driven. This local amplitude of forced free-stream oscillation was an order of magnitude greater than any unsteadiness which might have been induced inadvertently in the nominally steady flow which developed upstream.

4. Experimental results

4.1. *Preliminary considerations*

Experimental results are presented in which velocity and turbulence measurements, made in boundary layers with the same mean external conditions but with different time dependence, are compared. The time dependence corresponded to: (i) steady flow, (ii) quasi-steadily varying flow, and (iii) unsteady flow at different frequencies of mainstream unsteadiness. Quasi-steady measures were constructed from a series of 18 profiles of the steady boundary layer at the measurement station, recorded at approximately equal intervals over the range of free-stream velocities from $\langle u_\infty \rangle \approx U_0$ to $\langle u_\infty \rangle \approx U_0\,(1-2A)$. All data reported here were deduced from measurements made at the same station, with the same nominal amplitude of unsteadiness in the free stream.

The mean free-stream conditions for steady, quasi-steady and unsteady flow were matched at the same value of Clauser's equilibrium parameter β, defined as $(\delta^*/\tau_0)(\mathrm{d}P_\infty/\mathrm{d}x)$, which took the value of 6.3 for unsteady flow at this station. In the free stream,

$$\frac{1}{\rho}\frac{\mathrm{d}P_\infty}{\mathrm{d}x} \approx -\frac{1}{2}\frac{\mathrm{d}}{\mathrm{d}x}\left(U_\infty U_\infty + \overline{\tilde{u}_\infty \tilde{u}_\infty}\right), \tag{7}$$

and if steady and time-averaged unsteady boundary layers were compared only on the basis of their mean free-stream velocities, dissimilarity would be expected since the external pressure gradient would be lower when periodic velocities were present. Since it was desirable to have an appreciable amplitude of $\tilde{u}_\infty$ in this experiment, to assure a good signal-to-noise ratio in unsteady components of turbulence measures, the contributions of $\mathrm{d}(\overline{\tilde{u}_\infty \tilde{u}_\infty})/\mathrm{d}x$ to the mean pressure gradient were significant, amounting to nearly 9%. The exercise of matching profiles of steady and unsteady boundary layers with the same values of U_∞ was therefore inappropriate and likely to draw attention to features of the flow which were artifacts of the different pressure gradients present for steady and unsteady flow in this particular experiment, rather than effects due solely to mainstream unsteadiness. Therefore β was considered the appropriate matching parameter for steady and unsteady flow in this study. For the data of this study at $\beta = 6.3$, relative differences between the Reynolds numbers of the steady, quasi-steady and unsteady flows were negligible.

The response of the turbulent boundary layer to mainstream unsteadiness was studied at seven frequencies: 0.1, 0.2, 0.5, 0.8, 1.0, 1.6 and 2.0 Hz. The highest frequency in this range was of the order of $\bar{f}_\mathrm{B}$, the estimated average frequency at which rapid outward ejections of low-speed fluid (associated with a phase of the bursting phenomenon) would be detected in the steady turbulent boundary layer at

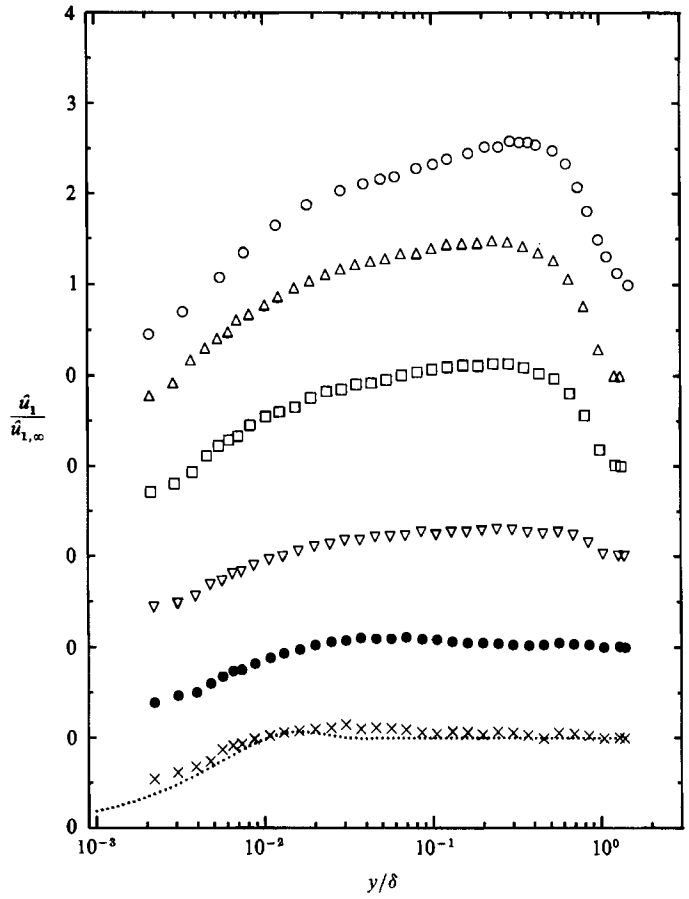

FIGURE 6. Boundary-layer profiles of $\hat{u}_1/\hat{u}_{1,\infty}$ *vs.* y/δ. · · · ·, Stokes' solution for oscillation at 2.0 Hz; ×, 2.0 Hz; ●, 1.0 Hz; ▽, 0.5 Hz; □, 0.2 Hz; △, 0.1 Hz; ○, quasi-steady flow.

the measurement station when the free stream was at its mean condition. An inner scaling deduced from the channel-flow data of Luchik & Tiederman (1987) ($u_\tau^2/[\nu \bar{f}_B] \approx 90$) implied this frequency would take a value of 3.6 Hz, whereas the outer scaling of Rao, Narasimha & Badri Narayanan (1971) ($U/[\delta^* \bar{f}_B] \approx 32$) gave a value of 1.8 Hz.

The behaviour of $\tilde{u}$ over the frequency range of this study is illustrated in figure 6, in which profiles of $\hat{u}_1$ (the amplitude of the first harmonic of $\tilde{u}$) are shown for a selection of frequencies. As $\hat{u}_1$ accounted for over 99% of the energy content of $\tilde{u}$, it could be considered quite representative of $\tilde{u}$. The abscissa in figure 6 is the wall-normal distance y scaled by the mean boundary-layer thickness δ and the ordinate normalization is by $\hat{u}_{1,\infty}$, the amplitude of modulation of the free stream. These variations in the amplitude of $\tilde{u}$ with frequency arise from the competing effects of the forcing oscillatory pressure gradient resisted by the inertia of the boundary-layer fluid; inertia dominates at low frequencies while the oscillatory pressure gradient governs high-frequency flow. These effects have been observed in many related experiments. The similarity between the quasi-steady profile and the one at 0.1 Hz indicated that the behaviour of $\tilde{u}$ at this frequency approached the asymptotic low-frequency response of $\tilde{u}$. Likewise, the profile of $\tilde{u}$ at 2.0 Hz is in good agreement with

the dotted line which represents the analytic solution of the Stokes equation (the asymptotic high-frequency form of the periodic x-momentum equation):

$$\frac{\partial \tilde{u}}{\partial t} = -\frac{1}{\rho}\frac{\partial \tilde{p}}{\partial x} + \nu \frac{\partial^2 \tilde{u}}{\partial y^2} \tag{8}$$

for the boundary conditions of this flow. Thus the upper limit of the frequency range corresponded to the asymptotic high-frequency response of $\tilde{u}$, which represents an oscillatory field of flow, the momentary condition of which departs significantly from its quasi-steady state. By inducing free-stream unsteadiness at frequencies of the order of the expected ejection frequency (representative of bursting events), and over a range which approached both the asymptotic high- and low-frequency responses of $\tilde{u}$, one may study the interaction between turbulence and organized unsteadiness ($\tilde{u}$) at timescales likely to be of importance to both the turbulence field and the periodic velocity field. In this paper, such interactions are examined mainly in a time-averaged sense.

Before presenting the results of this study, the scaling used for normalization of abscissas in subsequent graphs of experimental data is explained. Since wall units were the most appropriate kind, a reliable measure of the friction velocity in steady and time-averaged unsteady flow was sought. This measure was obtained from the linear region close to the wall ($y^+ \lesssim 7$, where $y^+ = yu_\tau/\nu$), within which the mean shear stress τ could be expressed as:

$$\tau = \mu \frac{\partial U}{\partial y} - \rho \overline{u'v'} - \rho \overline{\tilde{u}\tilde{v}}. \tag{9}$$

It differs from its form in steady flow by virtue of an additional stress due to organized oscillatory motions ($-\rho\overline{\tilde{u}\tilde{v}}$), which was negligible in the near-wall region of this flow (to be shown in §4.4). As is found in many steady flows, the influence of pressure gradient upon U was negligible so close to the wall, so a linear fit to the mean velocity profile was used to deduce u_τ. Details of this technique and its validation in steady and unsteady flow are described by Brereton (1989). It should be emphasized that although a log–linear fit (i.e. the Clauser technique) may yield a characteristic near-wall velocity scale when applied to profiles of U in time-averaged unsteady flow, it is not certain that this velocity scale is related to the wall shear through the well-known constants appropriate for steady flow.

4.2. *Time-averaged velocity profiles*

Boundary-layer profiles of U or $\overline{\langle u \rangle}$, normalized by their free-stream values, are shown in figure 7 for steady, quasi-steady and unsteady conditions (for which four representative frequencies within the range were selected) corresponding to $\beta = 6.3$. With the exception of some spread in the data close to the wall ($y/\delta \lesssim 0.01$), the collapse of all mean velocity profiles is excellent and no sensitivity to the different time histories of each data set is evident. It is important to note that this collapse was not achieved when steady and unsteady flows of the same free-stream velocity were compared, since their pressure gradients differed. The four profiles which describe the time-averaged response of U to sinusoidal unsteadiness are invariant with frequency – a result consistent with almost every study undertaken to date in this field. The steady and quasi-steady profiles of U/U_∞ are also virtually indistinguishable when compared at the same value of β. The excellent collapse of steady, quasi-steady and unsteady measurements of U/U_∞ at constant β (excepting

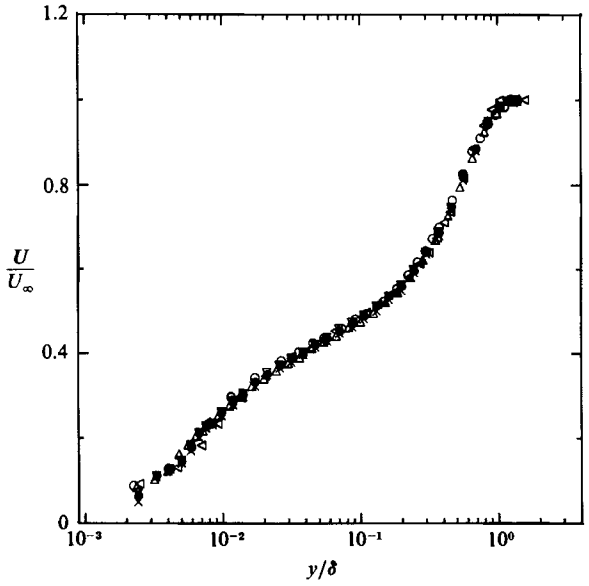

FIGURE 7. Boundary-layer profiles of U/U_∞ *vs.* y/δ. ◁, steady flow; ○, quasi-steady flow; △, 0.1 Hz; ▽, 0.5 Hz; ●, 1.0 Hz; ×, 2.0 Hz. For each profile $\beta = 6.3$.

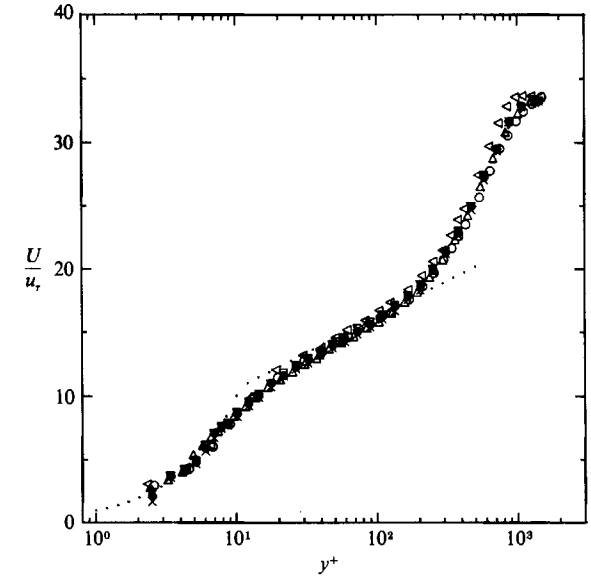

FIGURE 8. Boundary-layer profiles of U in wall units. · · · ·, $u^+ = y^+$, $u^+ = \frac{1}{0.41}\ln y^+ + 5.0$; ◁, steady flow; ○, quasi-steady flow; △, 0.1 Hz; ▽, 0.5 Hz; ●, 1.0 Hz; ×, 2.0 Hz. For each profile, $\beta = 6.3$.

near-wall discrepancies) was also found at neighbouring stations in this study and so $\partial U/\partial x$ could be considered invariant with the time history of the external flow (at least for $y/\delta \gtrsim 0.01$).

For each velocity profile shown in figure 7, the friction velocity was deduced using a near-wall linear fit and these data are replotted in wall units in figure 8. The mean friction velocity u_τ in steady and quasi-steady flow took values of 18.3 and 18.6 mm/s respectively and between 19.1 and 19.8 mm/s in the unsteady flows. Obviously, a

slightly better collapse of data is achieved for $3 < y^+ < 10$, though it is gained at the expense of a wider spread in data over the rest of the profile. It is important to note that the steady profile follows the log–linear portion of the law of the wall closely. This agreement could be taken as an indication that the inner region of the steady boundary layer was very close to its equilibrium state and was not undergoing any appreciable streamwise recovery in response to the effect of changes in the mean value of the external pressure gradient within the test section. The trend for quasi-steady and unsteady data is to fall a little below and at a slightly oblique angle to the line representing the log–linear variation of U in the steady turbulent boundary layer. Although it is possible that this result was an artifact of some systematic error in deducing u_τ, the same result was found for unsteady flow at other locations. Moreover when the linear fit was applied to each in the series of steady-flow profiles used to construct the quasi-steady one, its agreement with the Clauser technique (which is applicable for each steady-flow case) was always within $\pm 2\%$. Similar (and at some locations, larger) effects of this distortion of the log–linear region were noted when velocity data taken at neighbouring locations were normalized by inner variables (Brereton 1989). A small effect of imposing unsteadiness upon the flow is then to cause distortion of the log–linear region in this flow, when profiles of U are plotted in wall units. This finding is consistent with the results of the unsteady pipe-flow study of Tu & Ramaprian (1983) (in which they noted a small downward shift of the log–linear region) and appears to support their deduction that the nonlinearity of the streamwise momentum equation would account for local differences between values of U measured under steady, quasi-steady and unsteady states.

Profiles of V, the wall-normal component of mean velocity, were also measured at frequencies ranging from 0.1 to 2.0 Hz but are not shown in this paper. No dissimilarity in profiles was discerned at any frequency in this range and so measurements of V (and $\partial V/\partial y$) were also considered invariant to forced sinusoidal unsteadiness.

4.3. *Time-averaged turbulence profiles*

Although spatial variations of U and V (and thus quantities such as $V\partial U/\partial y$, $U\partial U/\partial x$, and $\nu\partial^2 U/\partial y^2$) appeared to be unaffected by the differing time histories of the imposed free-stream unsteadiness, these results could not be taken as an indication that spatial distributions of time-averaged turbulence measures (i.e. $\partial(\overline{u'u'})/\partial x, \partial(\overline{u'v'})/\partial y$) would necessarily be uninfluenced too, despite their dependence through the time-averaged momentum equation:

$$\frac{\partial}{\partial x_j}(U_i U_j) = -\frac{1}{\rho}\frac{\partial P}{\partial x_i} - \frac{\partial}{\partial x_j}(\overline{u_i' u_j'} + \overline{\tilde{u}_i \tilde{u}_j}) + \nu\frac{\partial^2 U_i}{\partial x_j \partial x_j}. \tag{10}$$

Without prior knowledge of the relative sizes of other terms in (10), direct measurement is necessary to establish conclusively whether $\overline{u_i' u_j'}$ exhibits any significant dependence upon frequency.

Profiles of $(\overline{u'u'})^{\frac{1}{2}}/u_\tau$ are shown in figure 9 for the same range of conditions over which the response of U was plotted in figures 7 and 8. The appearance of dual peaks in these profiles and the normalized levels of u' are in conformity with studies of steady turbulent boundary layers in adverse pressure gradients. The four profiles measured under conditions of sinusoidal unsteadiness exhibit invariance to frequency, consistent with findings of many other studies. This invariance was also observed in measurements of $\overline{v'v'}$, which are not shown. Furthermore, this same insensitivity to frequency variation was found at neighbouring stations in this study

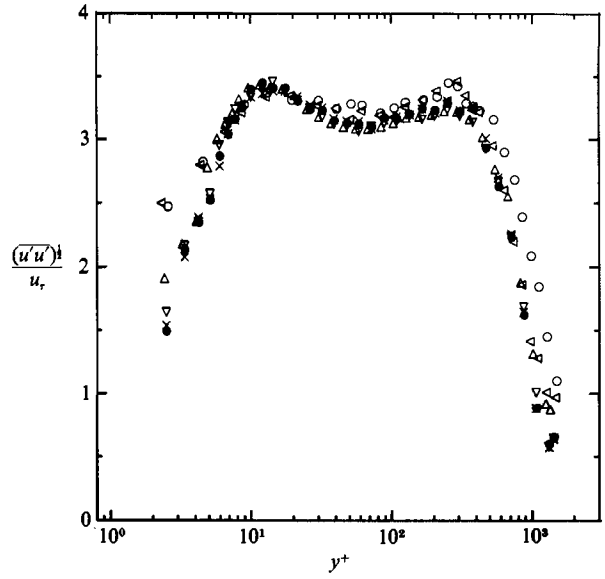

FIGURE 9. Boundary-layer profiles of $(\overline{u'u'})^{\frac{1}{2}}$ in wall units. ◁, steady flow; ○, quasi-steady flow; △, 0.1 Hz; ▽, 0.5 Hz; ●, 1.0 Hz; ×, 2.0 Hz. For each profile, $\beta = 6.3$.

and so $\partial(\overline{u'u'})/\partial x$ could be considered frequency invariant. The steady and quasi-steady profiles are of almost identical shape throughout the boundary layer. However, these profiles are slightly dissimilar to profiles of $(\overline{u'u'})^{\frac{1}{2}}$ measured under conditions of sinusoidal unsteadiness. The levels of streamwise turbulence in steady and quasi-steady flow are a little higher, particularly beyond the inner part of the boundary layer ($y^+ \approx 30$). The innermost measurement of $(\overline{u'u'})^{\frac{1}{2}}$ is also higher than its local unsteady-flow counterparts. One possible explanation of this observation is that the flow oscillation mechanism induced very small amplitude vibrations in the apparatus such that the position of the measuring volume relative to the wall varied with phase. An effect such as this might have resulted in biasing turbulence measurements to lower mean values very close to the wall.

The slight differences in shape of the steady and unsteady profiles also give the appearance that the unsteady profiles were taken at a slightly weaker pressure gradient. This explanation was discounted since we went to great lengths to ensure that values of β were indeed matched. It is also possible that the slightly increased values of boundary-layer turbulence in steady and quasi-steady flow result from the turbulence level in the free stream (Charnay, Mathieu & Comte-Bellot 1976), which was a little greater for steady and quasi-steady flow than for unsteady flow (possibly owing to a very slight deterioration in the cleanliness of screens upstream of the flow contraction during the course of the experiment). This explanation was supported by measurements made at neighbouring locations, at which the free-stream turbulence levels were closer in value in both steady and unsteady flow and discrepancies between profiles of $(\overline{u'u'})^{\frac{1}{2}}$ were lower. Since the slight discrepancies observed between steady and unsteady profiles of $(\overline{u'u'})^{\frac{1}{2}}$ might be accounted for by these experimental uncertainties, it could not be concluded that sinusoidal free-stream unsteadiness had any major effect upon the mean condition of the streamwise component of turbulence within the boundary layer.

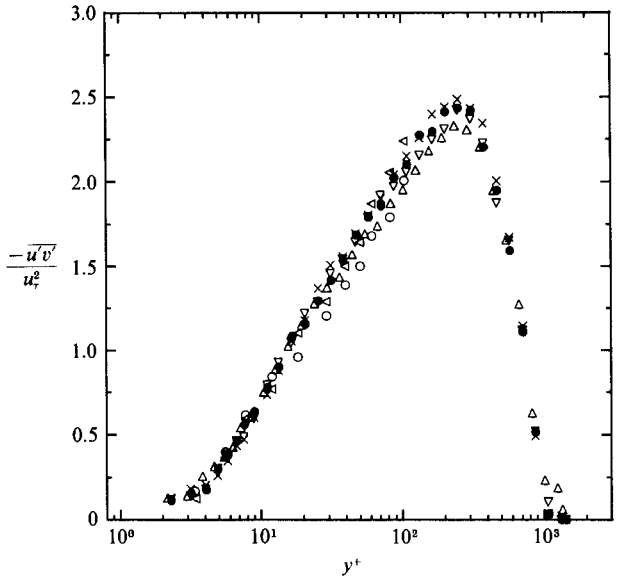

FIGURE 10. Boundary-layer profiles of $-\overline{u'v'}/u_\tau^2$. △, 0.1 Hz; ▽, 0.5 Hz; ●, 1.0 Hz; ×, 2.0 Hz; ◁, steady flow; ○, quasi-steady flow. For each profile, $\beta = 6.3$.

4.4 *Time-averaged profiles of Reynolds stresses*

The time-averaged momentum equation (10) contains two Reynolds-stress tensors, $\partial(\overline{u_i' u_j'})/\partial x_j$ and $\partial(\overline{\tilde{u}_i \tilde{u}_j})/\partial x_j$, which arise as a result of the triple decomposition and the averaging procedures described by (3), (4) and (5). Profiles of $-\overline{u'v'}$ were measured over the range of frequencies of forced unsteadiness and are shown in figure 10. It may be seen that $-\overline{u'v'}$ is insensitive to variation in the frequency of free-stream unsteadiness, which is consistent with the behaviour observed in profiles of U and $(\overline{u'u'})^{\frac{1}{2}}$. Unfortunately, measurements of $-\overline{u'v'}$ made under quasi-steady and steady conditions at this location were not available for comparison and their absence is a weakness of the present study. However, these missing data could be re-created artificially from the measured profiles of U and the shear-stress-to-velocity-gradient data of Andersen, Kays & Moffat (1975), for steady flow over a range of positive pressure gradients at comparable Reynolds numbers. These data are plotted in figure 10, though only as far from the wall as $y^+ = 100$. Beyond this point, the relative uncertainty in $\partial U/\partial y$ became sufficiently large that reasonably accuracy in $-\overline{u'v'}$ was no longer likely. Since these data match the unsteady measurements of $-\overline{u'v'}$ very closely, it appears most unlikely that sinusoidal free-stream unsteadiness has any major effect upon the mean condition of the turbulent Reynolds stress within the boundary layer.

The Reynolds stress $-\overline{\tilde{u}\tilde{v}}$ arises from the time-averaged correlation of oscillatory components of velocity. Since this stress is not present in the steady turbulent flow of this study, it is of great interest to compare its value in unsteady flow to values of quantities such as $-\overline{u'v'}$, which are common to both steady and unsteady flow. Profiles of $-\overline{\tilde{u}\tilde{v}}$ are shown in figure 11 for the range of frequencies of unsteadiness studied; they are presented in wall units for ease of comparison with measures of $-\overline{u'v'}$, for which a representative profile at 0.5 Hz (from figure 10) is included. Frequency invariance is observed as far from the wall as $y^+ \approx 60$, though effects of oscillation at different frequencies then become apparent. The no-slip condition and

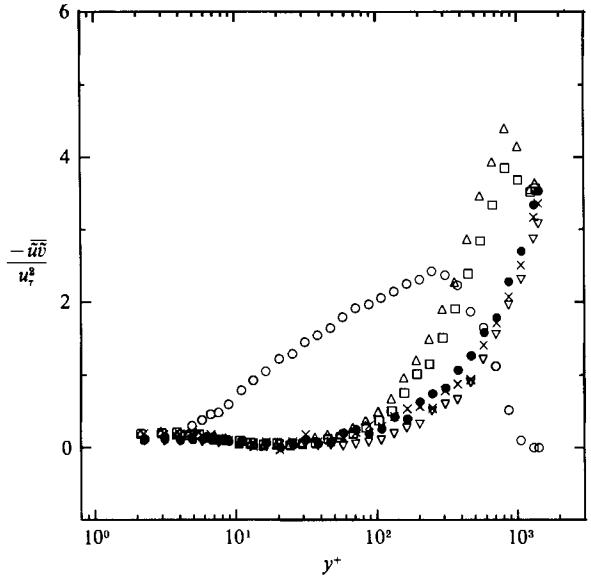

FIGURE 11. Boundary-layer profiles of $-\overline{\tilde{u}\tilde{v}}/u_\tau^2$. △, 0.1 Hz; □, 0.2 Hz; ▽, 0.5 Hz; ●, 1.0 Hz; ×, 2.0 Hz; ○, $-\overline{u'v'}/u_\tau^2$ at 0.5 Hz.

observance of continuity in the oscillatory field ($\partial\tilde{u}/\partial x + \partial\tilde{v}/\partial y = 0$, in nominally two-dimensional phase-averaged flow) require that the value of $-\overline{\tilde{u}\tilde{v}}$ is zero at the wall and that it has no gradient in the y-direction there. From figure 11 it is evident that these conditions are satisfied reasonably well (at least, relative to the magnitude and wall-normal gradient of $-\overline{u'v'}$). What could not be anticipated *a priori* was that the value of $-\overline{\tilde{u}\tilde{v}}$ would prevail almost at its value at the wall over a significant region of the boundary layer ($y^+ \leqslant 50$). Since $\tilde{u}$ was appreciable at all wall-normal positions at which measurements could be made, this is effectively a region within which $\tilde{v} \approx 0$. This observation was qualified by direct measurements of $\hat{v}_1$ (Brereton & Reynolds 1987) which indicated it was of the order of 1 % of $\hat{u}_{1,\infty}$ throughout this region. This result could be used to advantage, since $-\overline{u'v'}$ was also always a small percentage of $\nu\,\partial U/\partial y$ for $y^+ \lesssim 7$, and so τ_0 could be deduced from the linear fit to the profile of mean velocity suggested by (9) (Brereton 1989).

The frequency variation in measures of $-\overline{\tilde{u}\tilde{v}}$ is closely related to the frequency-dependent magnitude of $\tilde{u}$, shown in figure 6. At lower frequencies at which $\tilde{u}$ overshoots its free-stream value within the boundary layer, this stress attains significantly higher local values (say, for $200 < y^+ < 900$) than at the higher frequencies of the study, where slug-like flow in $\tilde{u}$ prevails. However, this organized stress, which represents the average of motions predominantly of the same single forcing frequency, plainly has little effect upon the turbulent Reynolds stress $-\overline{u'v'}$ (characterized by motions spanning a broad range of scales) since negligible variation of $-\overline{u'v'}$ with frequency is observed in figure 10. The organized and relatively unorganized Reynolds stresses do not appear to be coupled.

The wall-normal gradients of $-\overline{u'v'}$ and $-\overline{\tilde{u}\tilde{v}}$ play an additive role in the streamwise momentum equation (10), and so one might expect to observe some differences between the shapes of steady and unsteady profiles of U, owing to the enhanced value of their sum in the outer unsteady boundary layer. However the wall-normal gradients of both terms are much smaller than those of $-\overline{u'v'}$ close to the wall and

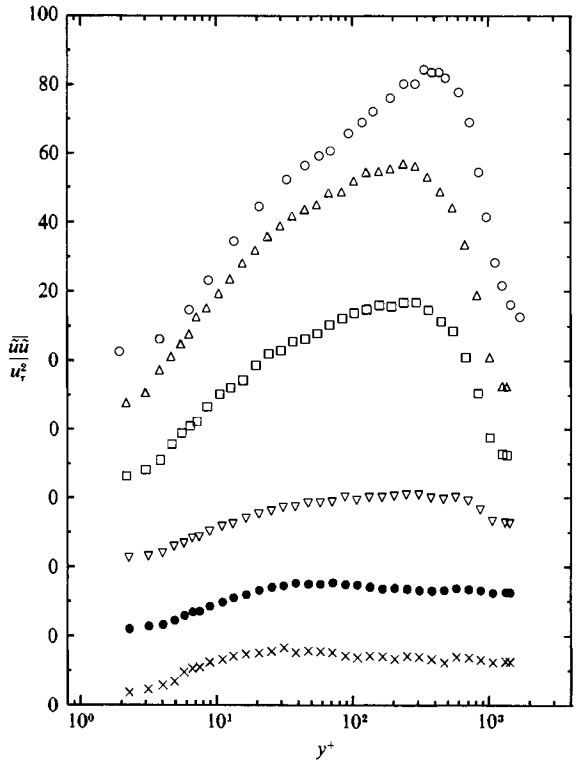

FIGURE 12. Boundary-layer profiles of $\overline{\tilde{u}\tilde{u}}/u_\tau^2$. ×, 2.0 Hz; ●, 1.0 Hz; ▽, 0.5 Hz; □, 0.2 Hz; △, 0.1 Hz; ○, quasi-steady flow.

the apparent collapse of measurements of U in figures 7 and 8 implies that effects of this additional Reynolds stress upon the shape of the U profile are very small ones at most.

The behaviour of $\overline{\tilde{u}\tilde{u}}$ is shown in figure 12 and, at different frequencies, variations in the magnitude of this quantity may be identified clearly. The streamwise derivative of this quantity could not be gauged accurately without undertaking a much greater number of measurements at different streamwise locations and so the question of whether the magnitude of $\partial(\overline{\tilde{u}\tilde{u}})/\partial x$ (and by a process of elimination of all other terms in (10), $\partial P/\partial x$) varied with frequency could not be addressed satisfactorily. However, from inspection of figure 12 it is apparent that, at different frequencies of unsteadiness, the local value of $\overline{\tilde{u}\tilde{u}}$ may vary between 10 times and 35 times the size of u_τ^2 in the region close to the wall ($y^+ \lesssim 30$), where one might expect interaction between organized unsteadiness ($\tilde{u}$) and the turbulence-producing motions of the boundary layer to be most pronounced. Yet from the data of figure 9, no corresponding variation with frequency is detectable in $\overline{u'u'}$ at all; $\overline{u'u'}$ remains insensitive to frequency effects and its value is typically a factor of ten larger than u_τ^2. Nor is there any variation with frequency in measurements of $-\overline{u'v'}$ shown in figure 10. These results are noteworthy as they indicate that the insensitivity of the turbulent motions associated with $\overline{u_i' u_j'}$ to the highly organized superimposed velocity field is such that, whether $\overline{\tilde{u}\tilde{u}}$ is of the same size as $\overline{u_i' u_j'}$ or nearly four times larger, no differences in $\overline{u_i' u_j'}$ are observed. In a time-averaged sense, the turbulent field appears uncoupled from the oscillatory one.

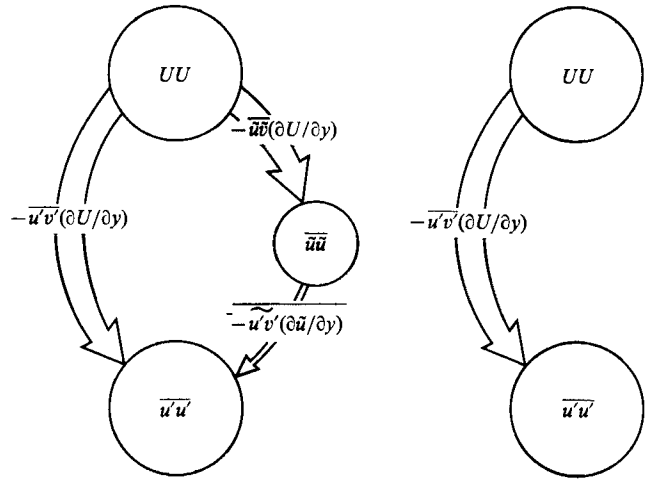

FIGURE 13. Transfer of kinetic energy between velocity fields close to the wall in steady and unsteady turbulent boundary layers. The arrow thickness represents the relative size of each participating term.

The frequency-dependent effects in time-averaged measurements of mean and turbulent quantities which have been revealed so far are those in $-\widetilde{\tilde{u}\tilde{v}}$ and $\widetilde{\tilde{u}\tilde{u}}$, the mean correlations of organized motions which result from the imposed oscillatory field, and the slight differences detected between profiles of U measured in steady and unsteady flow, when compared in wall units. While it seems likely that the slightly different profiles of U found for steady and unsteady flow should result from differences between steady and unsteady values of nonlinear terms of (10), it is not clear from this study which nonlinear terms account for this small difference. The sensitivity of U to subtle changes in gradients of the Reynolds-stress tensors (10) may well be sufficiently large that measurable differences in U are accounted for by differences in turbulence measurements which are indistinguishable from scatter in the reported data.

In summary, the mean turbulence field appears to be virtually unchanged from either its steady or quasi-steady states over the entire range of frequencies (0.1→ 2.0 Hz) imposed in this study. The turbulent motions of these boundary layers thus preserve the same average character, regardless of the timescale of the imposed mainstream disturbance and may be viewed as robust to different discrete frequencies of sinusoidal disturbance, of amplitudes which vary across the boundary layer. We examine this robust characterization of time-averaged turbulent motions of the boundary layer further by focusing on the quantity which describes their generation – the production tensor.

4.5. *Time-averaged and time-dependent production of turbulent kinetic energy*

The general invariance to frequency of disturbance noted in profiles of U, $\overline{u'u'}$ and $-\overline{u'v'}$ under steady, quasi-steady and sinusoidally unsteady conditions, may be interpreted more clearly through consideration of the corresponding levels of turbulence production. The additional velocity field ($\tilde{u}_t$) admitted by the triple decomposition of §3.2 enables energy transfer to be viewed as taking place between three participating fields, rather than only the mean and turbulent ones associated

with the conventional Reynolds decomposition. The set of differential equations describing transport of the mean squares of U_i, $\tilde{u}_i$ and u_i' may be deduced in component form, yielding the coupled time-averaged 'energy' equations:

$$\frac{\mathrm{D}}{\mathrm{D}t}(U_\alpha U_\alpha) = \ldots + \overline{u_i' u_\alpha'}\frac{\partial U_\alpha}{\partial x_i} + \overline{\tilde{u}_i \tilde{u}_\alpha}\frac{\partial U_\alpha}{\partial x_i} + \ldots, \tag{11}$$

$$\frac{\mathrm{D}}{\mathrm{D}t}(\overline{\tilde{u}_\alpha \tilde{u}_\alpha}) = \ldots + \overline{u_i' u_\alpha'\frac{\partial \tilde{u}_\alpha}{\partial x_i}} - \overline{\tilde{u}_i \tilde{u}_\alpha}\frac{\partial U_\alpha}{\partial x_i} + \ldots, \tag{12}$$

$$\frac{\mathrm{D}}{\mathrm{D}t}(\overline{u_\alpha' u_\alpha'}) = \ldots - \overline{u_i' u_\alpha'}\frac{\partial U_\alpha}{\partial x_i} - \overline{u_i' u_\alpha'\frac{\partial \tilde{u}_\alpha}{\partial x_i}} + \ldots, \tag{13}$$

where $\mathrm{D}/\mathrm{D}t$ denotes the substantial derivative following the organized motion of the fluid. In these equations, repeated Greek letters are used in subscripts when summation is not implied. Additional terms such as those describing pressure–strain, diffusion and dissipation in (13) are not written explicitly as we choose to focus on the production terms in this set of transport equations. The presence of two production terms in (13) is an artifact of the additional stage of decomposition employed, since they may be summed to yield the time average of the single phase-conditioned production tensor:

$$-\overline{u_i' u_\alpha'}\frac{\partial U_\alpha}{\partial x_i} - \overline{u_i' u_\alpha'\frac{\partial \tilde{u}_\alpha}{\partial x_i}} = -\overline{\left\langle u_i' u_\alpha' \frac{\partial \langle u_\alpha \rangle}{\partial x_i} \right\rangle}. \tag{14}$$

The representation as two distinct tensors is preferred as it allows the different interactions of the turbulence field with the mean and oscillatory fields to be identified clearly. The roles of the major terms of these production tensors are illustrated in figure 13, together with the role of the term found from the usual Reynolds decomposition, commonly used to describe steady turbulent flow. In particular, it may be seen that, on average, the action of the periodic velocity field upon the oscillatory component of the turbulent Reynolds stress accounts for energy exchange between the turbulent and oscillatory fields of flow. Without prior knowledge of the sizes of $-u_i' u_\alpha'$ and $\partial \tilde{u}_\alpha/\partial x_i$ and their phase relationship, one cannot be certain if this term represents a supply of energy to the turbulent field, or a loss of energy from it, or if it is of significance.

For the case of production of $\overline{u'u'}$, the largest component of the time-averaged Reynolds-stress tensor in this flow, estimates of the order of magnitude of the production terms of (13) were used to determine the major ones responsible for transfer of kinetic energy to the $\overline{u'u'}$ field. These terms were $-\overline{u'v'}\,\partial U/\partial y$ and $-\overline{\widetilde{u'v'}\,\partial \tilde{u}/\partial y}$ and they were measured at all frequencies of unsteadiness of this experiment. At each frequency $-\overline{u'v'}\,\partial U/\partial y$ was very much larger than $-\overline{\widetilde{u'v'}\,\partial \tilde{u}/\partial y}$. Thus nearly all energy transferred to the turbulent field was supplied directly from the mean flow, with only a small percentage transferred from the $\overline{\tilde{u}\tilde{u}}$ field. This finding is consistent with our view that, on average, the turbulent motions of the boundary layer are uncoupled from the periodic velocity field and thus insensitive to periodic shear at any single frequency with the range of this study. Since $-\overline{u'v'}\,\partial U/\partial y$ is of the same form as the term which accounts for most of the production of $\overline{u'u'}$ in steady turbulent boundary layers, it is interesting to examine whether the equivalence of $\overline{u'u'}$ in steady and unsteady flow is matched by equivalence in the major production term for $\overline{u'u'}$ under these conditions.

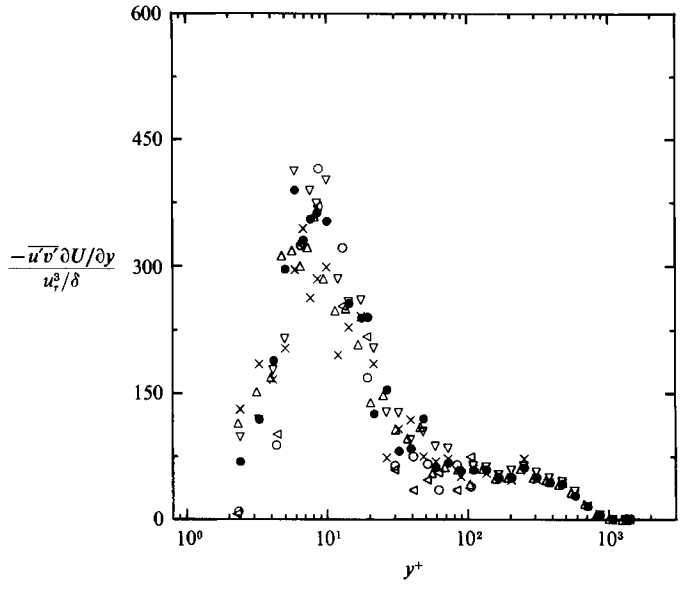

FIGURE 14. Boundary-layer profiles of $-\overline{u'v'}\,(\partial U/\partial y)/(u_\tau^3/\delta)$, the normalized form of the major production term for $\overline{u'u'}$. ◁, steady flow; ○, quasi-steady flow; △, 0.1 Hz; ▽, 0.5 Hz; ●, 1.0 Hz; ×, 2.0 Hz.

Profiles of $-\overline{u'v'}\,\partial U/\partial y$ are shown in figure 14, the normal gradient of U having been found from a piecewise-cubic spline fit to profiles of the streamwise velocity. As profiles of U and $-\overline{u'v'}$ (figures 8 and 10) are invariant to different frequencies of sinusoidal unsteadiness, it is not surprising that profiles of this production term show no obvious dependence upon frequency. Although there is considerable scatter in these data, the peaks of each profile are approximately coincident at $y^+ \approx 8$ and their magnitudes are all about $375u_\tau^3/\delta$. The steady and quasi-steady profiles of $-\overline{u'v'}\,\partial U/\partial y$ are also included in figure 14, having been deduced using the method described in §4.4. These profiles are in good overall agreement with the unsteady ones in both shape and magnitude, implying that the time-averaged effect of the dynamical motions associated with turbulence production in unsteady flow may be no different from that of its steady-flow counterpart. If this were the case, mechanisms of turbulence production could be viewed in a time-averaged sense as robust ones which, on average, are insensitive to disturbances at any single frequency within the range of this study.

The tensor describing time-dependent production of turbulent kinetic energy may be identified by considering the periodic energy budget, which accounts for temporal exchanges of turbulent kinetic energy about a mean level of zero, during any unsteady cycle. Just as mean production of $\langle u'_\alpha u'_\alpha \rangle$ is described by the time average of $-\langle u'_i u'_\alpha \partial \langle u_\alpha \rangle / \partial x_i \rangle$, its temporal component corresponds to the oscillatory part of this tensor and it may be shown that:

$$\frac{\mathrm{D}}{\mathrm{D}t}\widetilde{(u'_\alpha u'_\alpha)} = \ldots - \widetilde{\left\langle u'_i u'_\alpha \frac{\partial \langle u_\alpha \rangle}{\partial x_i} \right\rangle} + \ldots$$

$$= \ldots - \overline{u'_i u'_\alpha}\frac{\partial \tilde{u}_\alpha}{\partial x_i} - \widetilde{u'_i u'_\alpha}\frac{\partial U_\alpha}{\partial x_i} - \widetilde{u'_i u'_\alpha}\frac{\partial \tilde{u}\alpha}{\partial x_i} + \ldots \qquad (15)$$

In this equation the symbol $\widetilde{\ }$ has the same meaning as $\sim$; it denotes the periodic or oscillatory component of its argument – the momentary deviation of the phase average of a quantity from its time-averaged value. Since it is the role of the production tensors which is of prime concern, the time-dependent pressure-strain, diffusion and dissipation terms are given no explicit form.

Production of $\widetilde{u'u'}$, the largest component of the oscillatory Reynolds-stress tensor in this flow, was attributed predominantly to the quantity $-\widetilde{\langle u'v'\,\partial\langle u\rangle/\partial y\rangle}$ through order-of-magnitude reasoning. This tensor could be re-expressed as the sum of the three distinct tensors: $-\widetilde{u'v'}\,\partial U/\partial y$, $-\widetilde{u'v'}\,\partial\tilde{u}/\partial y$ and $-\widetilde{u'v'\,\partial\tilde{u}/\partial y}$. The third of these was very much smaller (at least an order of magnitude) than the first two, throughout the boundary layer at all frequencies of unsteadiness. Therefore production of $u'u'$ in the oscillatory field of flow could be characterized as predominantly due to the terms $-\widetilde{u'v'}\,\partial U/\partial y$ and $-\widetilde{u'v'}\,\partial\tilde{u}/\partial y$. The amplitudes of these two major contributors to production of $\widetilde{u'u'}$ were deduced from Fourier decomposition of phase-conditioned experimental data and each was most energetic at the forcing frequency throughout the boundary layer.

Profiles of the first Fourier amplitude of the sum of the three oscillatory production terms are shown in figure 15, at selected frequencies within the range of this study. They are plotted together with $-\widetilde{u'v'}\,\partial U/\partial y$, the major term accounting for production of $\widetilde{u'u'}$, at a representative frequency of 0.1 Hz. At this level of mainstream unsteadiness ($\hat{u}_{1,\infty} \approx 0.15U_\infty$), the amplitude of production of $u'u'$ is evidently of the order of the level of mean production of $\widetilde{u'u'}$ close to the wall. For quasi-steady flow, and for flow at low frequencies which approach this asymptote, time-dependent production of $u'u'$ varies between extremes of almost zero and nearly twice its mean level during each cycle. Although these data give the appearance that the amplitude of oscillatory production of $\langle u'u'\rangle$ may even exceed its mean level of production at 0.1 Hz, thereby implying momentary energy exchange from the turbulent field to the oscillatory one, the uncertainties inherent in the deduction of velocity gradients from numerical differentiation of discrete experimental data preclude placing much confidence in this observation.

The effect of increasing the frequency of the sinusoidal disturbance above its low-frequency asymptote is to decrease the amplitude of the oscillatory component of turbulence production (a detailed discussion of which will be reported elsewhere). The departure of the amplitude of this production measure from its quasi-steady state over the range of frequencies considered is again noteworthy. However, the significance to this paper of the data shown in figure 15 is that the measurements of mean and oscillatory production of $\langle u'u'\rangle$ are described by profiles of very similar shapes, with peaks coincident in space (around $y^+ \approx 8$). Since bursting processes in steady turbulent boundary layers result in the distinctive highly-localized near-wall peaks in $-\overline{u'v'}\,\partial U/\partial y$ (figure 14, Kline *et al.* 1967), a coincident peak of similar shape in the oscillatory field may be regarded as a modulation of the bursting process of the mean flow, rather than an independent facet of the oscillatory flowfield alone. This argument is reinforced by our finding that, of the three distinct tensors which sum to $-\widetilde{\langle u'v'\,\partial\langle u\rangle/\partial y\rangle}$, the one representing solely oscillatory components of organized and turbulent motions ($-\widetilde{u'v'\,\partial\tilde{u}/\partial y}$) was at least an order of magnitude smaller than either $-\widetilde{u'v'}\,\partial U/\partial y$ or $-\overline{u'v'}\,\partial\tilde{u}/\partial y$, each of which describe the product of a modulated quantity and a mean one. Thus the process of time-dependent production of new turbulence may well result from the superimposed oscillatory flow acting only to modulate the bursting process in the underlying mean flow, while preserving the

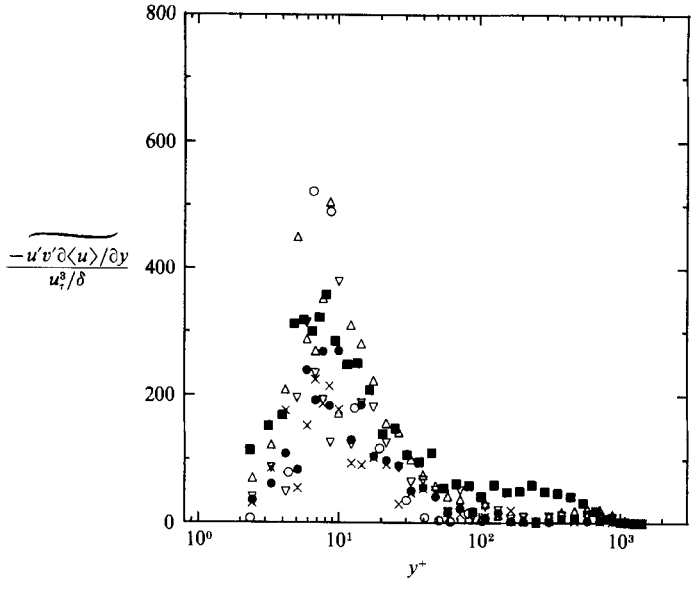

FIGURE 15. Boundary-layer profiles of $\widehat{-u'v'\partial\langle u\rangle/\partial y}/(u_\tau^3/\delta)$ at its first harmonic, the normalized amplitude of the production term for $\widehat{u'u'_1}$. ○, quasi-steady flow; △, 0.1 Hz; ▽, 0.5 Hz; ●, 1.0 Hz; ×, 2.0 Hz; ■, $-\overline{u'v'}(\partial U/\partial y)/(u_\tau^3/\delta)$, the normalized form of the major production term for $\overline{u'u'}$, at 0.1 Hz.

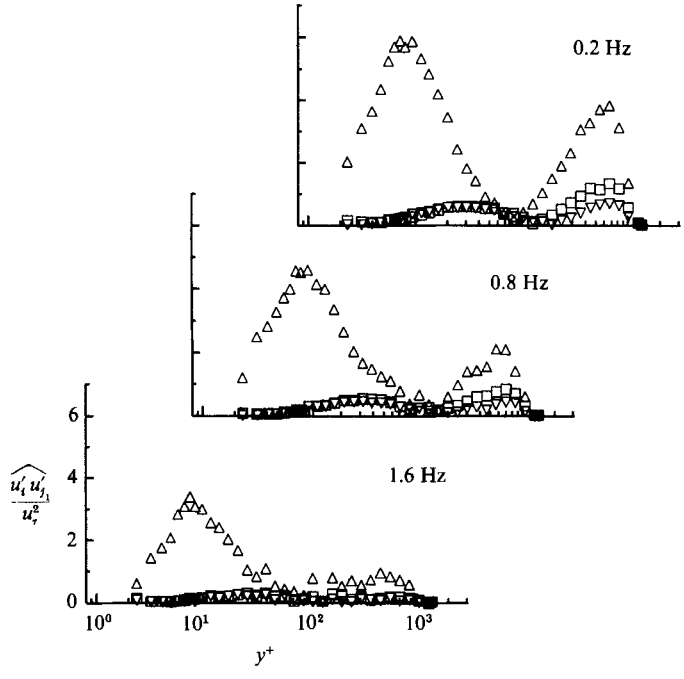

FIGURE 16. Boundary-layer profiles of the amplitude of oscillations in components of the Reynolds-stess tensor, normalized in wall units. Amplitudes are plotted at their first harmonics at 0.2, 0.8 and 1.6 Hz. △, $\widehat{u'u'_1}/u_\tau^2$, □, $\widehat{v'v'_1}/u_\tau^2$, ▽, $\widehat{u'v'_1}/u_\tau^2$.

same mean character of these turbulent motions. This notion is in conformity with results of the recent channel-flow study of Tardu *et al.* (1987) in which it was demonstrated that, when time-dependent burst detection (variable-interval time-averaging, conditioned on a specific phase of the bursting phenomenon) was referenced to the phase of the imposed unsteadiness, the phase-conditioned detection frequency was clearly modulated about its mean value.

The view that production of oscillatory measures of Reynolds stresses ($\widetilde{u_i' u_j'}$) arises as a consequence of modulation of the dynamical motions associated with turbulence production in the time-averaged field of flow has important implications concerning the wall-normal distribution of the oscillatory turbulence field. Close to the wall it should scale upon a measure of the mean flow such as y^+, rather than the frequency-dependent quantity $y/(\nu/\omega)^{\frac{1}{2}}$, appropriate for characterization of viscous diffusion in laminar flow. This view is supported by the data shown in figure 16, in which similarity is observed in profiles of the amplitudes of the first harmonics of $\widetilde{u'u'}$, $\widetilde{v'v'}$ and $-\widetilde{u'v'}$ when plotted as functions of y^+, an abscissa referenced to a lengthscale of the mean flow. Data are shown for three frequencies of unsteadiness, selected to be representative of measurements made over the range of frequencies considered. The spatial coincidence at $y^+ \approx 8$ of the near-wall peaks in $\widehat{u'u'}_1$, those of its production term (shown in figure 15) and those of $-\overline{u'v'}\,\partial U/\partial y$, the major term accounting for production of $\overline{u'u'}$ (in figure 14), conforms with the view that oscillatory measures of $u'u'$ arise primarily through modulation of the dynamical motions associated with turbulence production in the time-averaged field of flow. Other details of the temporal behaviour of the turbulence field, as represented by these components of the oscillatory Reynolds-stress tensor, will be reported separately.

The findings of this section which concern turbulence production are necessarily restricted to inferences drawn from time- and phase-averages of measurable features of the flow. The possibilities for gaining clearer insight into the temporal nature of the dynamical motions linked to turbulence production (under conditions of forced unsteadiness) are restricted by the difficulties inherent in acquiring spatio-temporal information very close to the wall. Information of this kind could not be deduced in this study and its measurement and interpretation remains a research challenge for the future.

4.6. *Time-dependent diffusion of vorticity*

We conclude presentations of experimental results by returning to the theme of interpreting effects of imposed unsteadiness upon turbulent boundary layers in terms of the resulting distribution of spanwise vorticity. In unsteady boundary layers, the pressure gradient imposed in the free stream generates a flux of unsteady spanwise vorticity which diffuses from the wall, where the temporal behaviour of the spanwise vorticity is described by (1). Away from the wall, $-\partial\tilde{u}/\partial y$ could still be considered the major contributor to ω_3 and its behaviour was deduced from phase-averaged profiles of $\langle u \rangle$. At each discrete phase, ensemble-averaged measures of streamwise velocity were differentiated in the y-direction by fitting a piecewise-cubic spline to these data. The oscillatory component of velocity gradient was then expressed as $\widehat{\partial\tilde{u}/\partial y}_1$, the Fourier amplitude of $\partial\tilde{u}/\partial y$ at the forcing frequency. Since the harmonic content at the fundamental frequency exceeded 97 % of the total harmonic content of $\tilde{u}$ at every measurement position within the boundary layer, at each forcing frequency, $\partial\tilde{u}/\partial y$ could be described adequately by $\widehat{\partial\tilde{u}/\partial y}_1$ and an accompanying phase measure. Therefore $\widehat{\partial\tilde{u}/\partial y}_1$ was taken as the amplitude of oscillatory spanwise vorticity $\tilde{\omega}_3$.

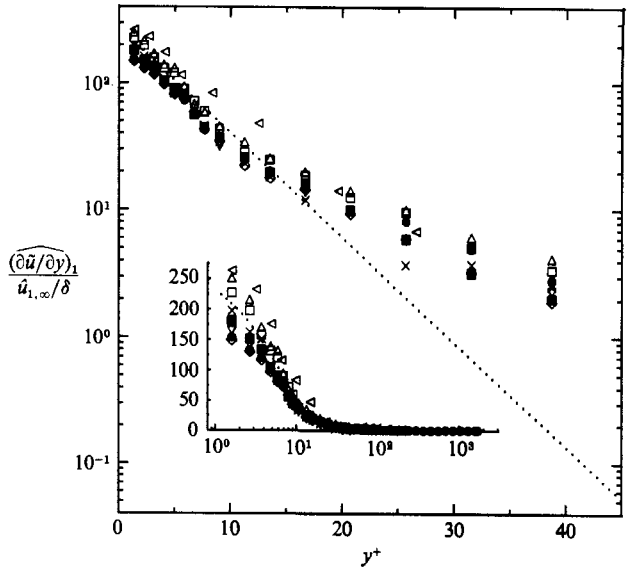

FIGURE 17. Near-wall distribution of $\widehat{(\partial\tilde{u}/\partial y)}_1/(\hat{u}_{1,\infty}/\delta)$, the first harmonic of normalized oscillatory shear. · · · ·, Stokes' solution for oscillation at 2.0 Hz; ×, 2.0 Hz; ■, 1.6 Hz; ●, 1.0 Hz; ◇, 0.8 Hz; ▽, 0.5 Hz; □, 0.2 Hz; △, 0.1 Hz; ◁, quasi-steady flow. The inset figure shows this distribution over the entire boundary layer.

Distributions of $\widehat{\partial\tilde{u}/\partial y_1}$ within the boundary layer are shown in figure 17, for the range of frequencies studied in this experiment. The scatter introduced by differentiation of $\langle u\rangle$ data appears to be as great as any effect of frequency, and must mask the subtle differences in the true shapes of these profiles which account for the strong frequency dependence exhibited by measures of $\tilde{u}$ in figure 6. The data of figure 17 appear reasonably well grouped around the high-frequency asymptote for $\widehat{\partial\tilde{u}/\partial y_1}$, described by the quasi-laminar analytical solution to the oscillatory x-momentum equation (8). This analytical representation is plotted for oscillation at 2.0 Hz, just as the corresponding description of $\tilde{u}$ was plotted in figure 6. For the case of a stationary wall and an oscillatory free stream, this asymptotic solution for $\widehat{\partial\tilde{u}/\partial y_1}$ takes the form:

$$\frac{\widehat{\partial\tilde{u}}}{\partial y_1} = \frac{\hat{u}_{1,\infty}}{(\nu/\omega)^{\frac{1}{2}}} e^{-y/(2\nu/\omega)^{\frac{1}{2}}}. \tag{16}$$

The normalization chosen for the ordinate of figure 17 is $\hat{u}_{1,\infty}$ (or $U_0 A$ using the nomenclature of (2)) divided by the mean boundary-layer thickness δ, rather than by the frequency-dependent Stokes thickness $(\nu/\omega)^{\frac{1}{2}}$. Since the mean value of δ was virtually unchanged from its steady-flow value by either quasi-steady or unsteady oscillation in this experiment, its use allowed direct comparison of amplitudes of the oscillatory component of vorticity in a dimensionless form.

From figure 17 it may be seen that the decay in amplitude of $\tilde{\omega}_3$ in the wall-normal direction is very similar for all frequencies of unsteadiness, when plotted in wall units. The oscillatory spanwise vorticity equation for this two-dimensional (phase-averaged) flow may be written as:

$$\frac{\partial\tilde{\omega}_3}{\partial t} + U\frac{\partial\tilde{\omega}_3}{\partial x} + V\frac{\partial\tilde{\omega}_3}{\partial y} + \tilde{u}\frac{\partial\Omega_3}{\partial x} + \tilde{v}\frac{\partial\Omega_3}{\partial x} = \frac{\partial}{\partial x_j}\left(u_3'\omega_j' - \omega_3' u_j'\right) + \nu\frac{\partial^2\tilde{\omega}_3}{\partial y^2}. \tag{17}$$

In the asymptotic case of high-frequency flow, the turbulent and convective terms in (17) play no role. However, at lower frequencies of oscillation, when these terms do become important, with the exception of a few very-near-wall data all $\tilde{\omega}_3$ profiles appear to decay with increasing y^+ in roughly the same manner with no obvious dependence upon frequency. The region over which $\tilde{\omega}_3$ is most significant is restricted to $y^+ \lesssim 20$ and at any position within this region it is of comparable order at all frequencies considered.

The region extending outward from the wall as far as $y^+ \sim 20$ may usually be considered a Couette-flow region for mean flow in a steady turbulent boundary layer and the data presented in §4.4 indicate that it is also a region of parallel flow for the oscillatory velocity field. Thus if the flow may be considered a parallel one in both the mean and the oscillatory velocity fields for $y^+ \lesssim 20$ then all convective terms of (17) may be set to zero in this thin wall layer, leaving only the viscous term and the oscillatory component of the turbulent transport term to account for the outward decay in amplitude of $\tilde{\omega}_3$. Although these terms could not be measured in this study, it is reasonable to assume that turbulent motions dominate wall-normal diffusion of $\tilde{\omega}_3$ in the outer part of this wall layer. Using the kinematic identity: $\omega'_p u'_q - \omega'_q u'_p = \epsilon_{ipq}\{\partial(u'_i u'_j)/\partial x_j - \frac{1}{2}\partial(u'_j u'_j)/\partial x_i\}$, the turbulent transport term in (17) may be re-expressed in terms of second spatial derivatives of $\widetilde{u'u'}$, $\widetilde{v'v'}$ and $-\widetilde{u'v'}$, each of which scaled upon an abscissa referenced to y^+ (in figure 16). The association of the oscillatory turbulent transport term and the wall-normal distribution of $\widetilde{\partial u/\partial y_1}$ with a wall-normal lengthscale referenced to the mean flow, in contrast to the characterization of viscous diffusion by the frequency-dependent lengthscale $(\nu/\omega)^{\frac{1}{2}}$, indicates the dominance of turbulent transport in determining the wall-normal behaviour of $\tilde{\omega}_3$ over much of this thin near-wall layer. Thus the turbulent motions of this near-wall region do exhibit some coupling to this organized oscillatory shearing, but only in the sense that they act to confine it to the same region of influence, regardless of its prescribed timescale.

5. Concluding remarks

In this study, we have compared a turbulent boundary layer developing in steady flow with one developing under the same average external conditions, only with an additional oscillatory velocity field superimposed after that turbulent boundary layer was well established. Our results indicate, within experimental uncertainty, that mean statistical descriptions of turbulent motions of both kinds of boundary layer are equivalent, over a broad range of frequencies of unsteadiness. This equivalence in time-averaged measures was found for quasi-steady flow and for sinusoidal variation in free-stream velocity, even at frequencies for which the momentary condition of the organized velocity field differed substantially from its quasi-steady state. These finding are in conformity with results of several previous studies which featured boundary-layer initiation, transition and development under unsteady conditions, thereby implying that these characterizations are features of boundary-layer turbulence *per se* and not just of boundary layers which are initiated and undergo transition to turbulence under unsteady conditions.

The insensitivity of mean turbulence measures to sinusoidal disturbance is consistent with the view of turbulence as a broadband phenomenon, any mean measure of which comprises the summed contributions of a continuous range of scales of motion. Excitation at a single frequency within a broad range is therefore unlikely to have a noticeable effect upon an averaged measure of all scales of motion,

unless that discrete frequency happens to cause resonance or some other profound response within the boundary layer. In this study no such effects were observed. Although the highest frequencies of unsteadiness considered were of the order of the estimated ejection frequency (as associated with a phase of the bursting phenomenon), its true value could not be measured and questions concerning effects of flow oscillation at this frequency could not be addressed satisfactorily. The only coupling observed between the time-averaged turbulence field and the organized oscillatory one was the effectiveness of turbulent motions in confining the region over which oscillatory shear was significant to the same thin layer at the wall ($y^+ \lesssim 20$ in this study), regardless of the timescale of oscillation.

Measurements of the key terms describing production of new turbulence were very similar in the steady and the mean unsteady flows. Nor is there any evidence of new turbulence generated in significant quantities as a time-averaged effect of oscillatory motions alone. We are therefore led to believe that the dominant mechanisms for production of turbulence in these unsteady turbulent boundary layers cannot differ greatly from those in the steady boundary layer. When coupled with the comparability of mean velocity and mean components of the Reynolds-stress tensor in steady and unsteady flow, over the entire the boundary layer, this similarity in mean turbulence production implies that the motions in the thin wall region also play the same dominant role in determining the mean structure of the entire unsteady boundary layer as they are commonly believed to do in steady flow. It also indicates that, on average, the mechanisms of turbulence production are robust to disturbances in oscillatory velocity and shear fields (shear being most significant in the thin-wall region where mechanisms of turbulence production are most important) at any single frequency within the range of this study.

While the processes which result in turbulence production in the time-averaged field of flow appear resilient to oscillatory disturbance, local modulation of these processes seems to account for almost the entire production of turbulence in the oscillatory field. The profiles of the major oscillatory component of the turbulence-production tensor were very similar in shape to those of the primary term of the mean production tensor, with peaks at coincident positions in the thin near-wall region, indicating that time-dependent variations in the level of turbulence production could well arise from a local modulation of the dynamical motions which contribute to the time-averaged production process. The negligibly small measurements of the component of the oscillatory turbulence-production tensor arising from periodic shear acting upon the oscillatory component of turbulent shear stress – a facet of the oscillatory field alone – support this view.

Thus it appears that the near-wall motions of the boundary layer can withstand effects of oscillatory shear, which modulated turbulence production, yet these motions still maintain the same averaged statistical conditions throughout the boundary layer. These observations are interpreted as an indication of the rugged structures which develop in this thin near-wall region. This preservation of the mean near-wall structure, regardless of the timescales of oscillation imposed in this study, bears an interesting relation to some findings of Maruyama & Tanaka (1987) concerning effects of physical intrusion upon the structure of wall turbulence. In their experiment in which a wall-bounded turbulent flow was constrained by an array of spanwise fences, which were translated with the flow and protruded from the mainstream towards the wall, the near-wall structure could only be disturbed by the interference from these fence tips when they were positioned closer to the wall than $y^+ = 45$. Their findings concerning the toughness of the structure of wall turbulence

when exposed to periodic physical interference complement our finding of robustness to oscillatory disturbance; they reinforce our view of the near-wall motions of the turbulent boundary layer as most resilient to periodic external disturbance.

This study was carried out under US Army Research Office Grant DAAG 29-83-K-0056 and the authors gratefully acknowledge this support.

REFERENCES

ACHARYA, M. & REYNOLDS, W. C. 1975 Measurements and predictions of a fully developed turbulent channel flow with imposed controlled oscillations. *Report TF*-8, Department of Mechanical Engineering, Stanford University, Stanford, California.

ANDERSEN, P. S., KAYS, W. M. & MOFFAT, R. J. 1975 Experimental results for the transpired turbulent boundary layer in an adverse pressure gradient. *J. Fluid Mech.* **69**, 353–375.

BINDER, G., TARDU, S., BLACKWELDER, R. F. & KUENY, J. L. 1985 Large amplitude periodic oscillations in the wall region of a turbulent channel flow. *Proc. Fifth Symposium on Turbulent Shear Flows*, pp. 16.1–16.7. Cornell University, Ithaca, New York.

BLONDEAUX, P. & COLOMBINI, M. 1985 Pulsatile turbulent pipe flow. *Proc. Fifth Symposium on Turbulent Shear Flows*, pp. 16.15–16.21. Cornell University, Ithaca, New York.

BRERETON, G. J. 1989 Deduction of skin friction by Clauser technique in unsteady turbulent boundary layers. *Exp. Fluids* **7**, 422–424.

BRERETON, G. J. & REYNOLDS, W. C. 1987 Experimental study of the fluid mechanics of unsteady turbulent boundary layers. *Report TF*-29, Department of Mechanical Engineering, Stanford University, Stanford, California.

CEBECI, T. 1977 Calculation of unsteady two-dimensional laminar and turbulent boundary layers with fluctuations in external velocity. *Proc. R. Soc. Lond.* A **335**, 225–238.

CHARNAY, G., MATHIEU, J. & COMTE-BELLOT, G. 1976 Response of a turbulent boundary layer to random fluctuations in the external stream. *Phys. Fluids* **19**, 1261–1272.

COLES, D. E. 1968 The young person's guide to the data. *Proc. Computation of Turbulent Boundary Layers – 1968 AFOSR-IFP-Stanford conference*, vol. 2 Department of Mechanical Engineering, Stanford University, Stanford, California.

COUSTEIX, J. & HOUDEVILLE, R. 1983 Couches limites instationnaires. *Rapport Technique* 53/2259 and, Department d'Etudes et de Recherches en Aerothermodynamique, Centre d'Etudes et de Recherches de Toulouse, Toulouse.

HUSSAIN, A. K. M. F. & REYNOLDS, W. C. 1970 The mechanics of an organized wave in turbulent shear flow. *J. Fluid Mech.* **41**, 241–258.

JAYARAMAN, R., PARIKH, P. & REYNOLDS, W. C. 1982 An experimental study of the dynamics of an unsteady turbulent boundary layer. *Report TF*-18, Department of Mechanical Engineering, Stanford University, Stanford, California.

KARLSSON, S. K. F. 1959 An unsteady turbulent boundary layer. *J. Fluid Mech.* **5**, 622–636.

KEBEDE, W., LAUNDER, B. E. & YOUNIS, B. A. 1985 Large-amplitude periodic pipe flow: a second-moment closure study. *Proc. Fifth Symposium on Turbulent Shear Flows*, pp. 16.23–16.29. Cornell University, Ithaca, New York.

KENISON, R. C. 1977 An experimental study of the effect of oscillatory flow on the separation region in a turbulent boundary layer. *AGARD Conf. Proc.* 277 **20**.

KLINE, S. J., REYNOLDS, W. C., SCHRAUB, F. A. & RUNSTADLER, P. W. 1967 The structure of turbulent boundary layers. *J. Fluid Mech.* **30**, 741–773.

LIGHTHILL, M. J. 1954 The response of laminar skin friction and heat transfer to fluctuations in the stream velocity. *Proc R. Soc. Lond.* A **224**, 1–23.

LUCHIK, T. S. & TIEDERMAN, W. G. 1987 Timescale and structure of ejections and bursts in turbulent channel flows. *J. Fluid Mech.* **174**, 529–552.

MARUYAMA, S. & TANAKA, T. 1987 The effect of spatial restriction on the inner-layer structure of wall turbulence. *J. Fluid Mech.* **177**, 485–500.

MIZUSHINA, T., MARUYAMA, T. & HIRASAWA, H. 1975 Structure of the turbulence in pulsating pipe flows. *J. Chem. Engng Japan* **8**, 210–216.

MIZUSHINA, T., MARUYAMA, T. & SHIOZAKI, Y. 1973 Pulsating turbulent flow in a tube. *J. Chem. Engng Japan* **6**, 487–494.

PATEL, M. H. 1975 On laminar boundary layers in oscillatory flow. *Proc. R. Soc. Lond.* A **347**, 99–123.

PATEL, M. H. 1977 On turbulent boundary layers in oscillatory flow. *Proc. R. Soc. Lond.* A **353**, 121–144.

RAMAPRIAN, B. R. & TU, S. W. 1983 Fully developed periodic turbulent pipe flow. Part 2. The detailed structure of the flow. *J. Fluid Mech.* **137**, 59–81.

RAO, K. N., NARASIMHA, R. & BADRI NARAYANAN, M. A. 1971 The 'bursting' phenomenon in a turbulent boundary layer. *J. Fluid Mech.* **48**, 339–352.

SCHACHENMANN, A. A. & ROCKWELL, D. O. 1976 Oscillating turbulent flow in a conical diffuser. *Trans. ASME I: J. Fluids Engng* **98**, 695–701.

SIMPSON, R. L., SHIVAPRASAD, B. G. & CHEW, Y. T. 1983 The structure of a separating turbulent boundary layer. Part 4. Effects of periodic free-stream unsteadiness. *J. Fluid Mech.* **127**, 219–261.

TARDU, S., BINDER, G. & BLACKWELDER, R. 1987 Modulation of bursting by periodic oscillations imposed on channel flow. *Proc. Sixth Symposium on Turbulent Shear Flows*, pp. 4.5.1–4.5.6. Université Paul Sabatier, Toulouse.

TU, S. W. & RAMAPRIAN, B. R. 1983 Fully developed periodic turbulent pipe flow. Part 1. Main experimental results and comparison with predictions. *J. Fluid Mech.* **137**, 31–58.